Journal of Materials Chemistry A

COMMUNICATION

View Article Online
View Journal | View Issue

A hybrid lead iodide perovskite and lead sulfide QD heterojunction solar cell to obtain a panchromatic response

Cite this: *J. Mater. Chem. A*, 2014, **2**, 11586

Received 29th May 2014
Accepted 7th June 2014

DOI: 10.1039/c4ta02711f

www.rsc.org/MaterialsA

Lioz Etgar,*[a] Peng Gao,[b] Peng Qin,[b] Michael Graetzel[b] and Mohammad Khaja Nazeeruddin*[b]

We report for the first time on co-sensitization between $CH_3NH_3PbI_3$ perovskite and PbS quantum dots (QDs) in a heterojunction solar cell to obtain a panchromatic response from the visible to near IR regions. Following the deposition of the sensitizers on a TiO_2 film, an Au thin layer is evaporated on top as a back contact. Importantly, the $CH_3NH_3PbI_3$ nanoparticles and the PbS QDs used here simultaneously play both the role of a light harvester and a hole conductor, rendering superfluous the use of an additional hole transporting material. The mesoscopic $CH_3NH_3PbI_3$ (perovskite)–PbS (QD)/TiO_2 heterojunction solar cell shows an impressive short circuit photocurrent (J_{sc}) of 24.63 mA cm^{-2}, much higher than those of the individual $CH_3NH_3PbI_3$ perovskite and the PbS QD solar cells. The advent of such co-sensitization mesoscopic heterojunction solar cells paves the way to extend the absorbance region of the promising low cost, high-efficiency perovskite based solar cells.

Introduction

Recently, the methylammonium lead iodide perovskite has been shown as an excellent absorber, hole and electron transporting material useful for semiconductor and thin film photovoltaic applications.[1,2] The advantages of hybrid organic–inorganic methylammonium lead halide perovskites are large absorption coefficient, high charge carrier mobility and diffusion lengths.[3–10] Using methylammonium lead iodide perovskite as a light harvester, and 2,2′,7,7′-tetrakis(*N*,*N*-di-*p*-methoxyphenylamine)-9,9′-spirobifluorene (spiro-MeOTAD) as a hole transporting material, power conversion efficiencies (PCEs) of over 16% were obtained with both mesoporous metal oxide scaffolds and planar heterojunction architectures.[11–14] The ease with which these organic–inorganic hybrid perovskite materials can be prepared and processed from solution[3–13] whilst simultaneously providing desired device characteristics has made them an attractive alternative for thin film photovoltaics. Lee *et al.*[4] showed that a mixed-halide perovskite on a mesoporous Al_2O_3 photoanode acts both as a light absorber and an electron conductor. We have shown that the pure iodide perovskite can act as a hole conductor.[7,15] This demonstrates the interesting properties of perovskites in that they not only act as light absorbers but participate in the charge conduction.

However, the absorption onset of the $CH_3NH_3PbI_3$ perovskite is limited to 1.57 eV. Therefore, an effective approach to further increase the spectral response of these materials is co-sensitization with near IR absorbing nanoparticles. In the co-sensitization approach two or more sensitized materials combined absorb light.

Near IR Quantum Dots (QDs) have been used in several solar cell architectures such as QD-Schottky barrier solar cells, QD–polymer hybrid solar cells, QD–sensitized titanium dioxide (TiO_2) solar cells, and QD hybrid bilayer solar cells.[16–25] Efficiencies of 5–7% were achieved.[26–35]

Here we report for the first time on the co-sensitization between organo lead-halide perovskite and PbS QDs in a heterojunction solar cell. In this unique structure both the perovskite and the QDs were used as sensitizers and at the same time as hole conductors. The function of each material separately as a sensitizer and at the same time as a hole conductor in a heterojunction solar cell has already been proved in previous reports.[7,15] The J_{sc} of the co-sensitized devices was significantly enhanced relative to their corresponding single-sensitized devices, improving the overall performance for the $CH_3NH_3PbI_3$ perovskite + PbS QD device by 18% with respect to the $CH_3NH_3PbI_3$ devices.

Results and discussion

Fig. 1A shows a scheme of the co-sensitization of $CH_3NH_3PbI_3$ with the PbS QDs on a 500 nm TiO_2 film. The PbS QDs used in this study were with their original ligands, oleic acid, and they had the 1st excitonic peak at 920 nm wavelength corresponding

[a]*Institute of Chemistry, The Hebrew University of Jerusalem, Jerusalem 91904, Israel. E-mail: Lioz.etgar@mail.huji.ac.il*

[b]*Laboratoire de Photonique et Interfaces, Institut des Sciences et Ingénierie Chimiques, École Polytechnique Fédérale de Lausanne (EPFL), Switzerland. E-mail: mdkhajanazeeruddin@epfl.ch*

to E_g of 1.38 eV. The synthesis of $CH_3NH_3PbI_3$ and its deposition on the mesoporous TiO_2 film were carried out by spin coating of a 40 wt% precursor solution of CH_3NH_3I and PbI_2 in γ-butyrolactone. Upon drying at room temperature the film coated onto the TiO_2 film darkened in color, indicating the formation of $CH_3NH_3PbI_3$ in the solid state. The ionic and covalent interactions between the metal cations and the halogen anions create inorganic octahedra, while the cationic alkylammonium head groups provide charge balance to the structure.

The $CH_3NH_3PbI_3$ coated TiO_2 electrode was then deposited on the PbS QDs using a spin-coating method. Finally gold was evaporated as the back contact of the device. Fig. 1B shows a schematic energy level diagram of the hybrid $CH_3NH_3PbI_3$–PbS QD heterojunction solar cell. Upon illumination the $CH_3NH_3PbI_3$ perovskite and the PbS QDs absorb light, as a result electrons can travel in three possible channels, (i) electron injection from the $CH_3NH_3PbI_3$ perovskite to the TiO_2, (ii) electron injection from the PbS QDs to the TiO_2 and (iii) an electron transfer from the $CH_3NH_3PbI_3$ perovskite to the PbS QDs. Fig. 2A shows the absorption spectra of the $CH_3NH_3PbI_3$ perovskite and the PbS QDs on TiO_2 films, and the co-sensitization absorption spectra of the $CH_3NH_3PbI_3$ perovskite + 3 layers of PbS QDs. The PbS QDs have an absorption in the NIR region, while the absorption of the $CH_3NH_3PbI_3$ goes only up to 800 nm wavelength. The absorption of the co-sensitization system shows both contributions from the $CH_3NH_3PbI_3$ and the PbS QDs.

Further proof for the light harvesting contribution from both sensitizers can be observed in the emission spectra shown in Fig. 2B. All measurements were done on the Al_2O_3 substrate in order to use a similar morphology as the TiO_2 and at the same time to make sure that no injection of electrons will occur. In the case of the PbS QDs the emission peak can be recognized around 1100 nm, and for the $CH_3NH_3PbI_3$ perovskite the emission peak can be observed around 760 nm. In the case of the hybrid $CH_3NH_3PbI_3$ perovskite + 3 layers of PbS QDs both emission peaks can be seen clearly which suggest the activity of both materials in the hybrid structure. Interestingly, quenching of the emission spectra at 760 nm wavelength can be observed upon adding the PbS QD layers. On the other hand the emission at 1100 nm wavelength, which belongs to the PbS QDs, does not decrease, suggesting energy transfer from perovskite to PbS QDs.

In order to find the best co-sensitization system we tried to deposit different numbers of QD layers on top of the perovskite. The photovoltaic parameters for the $CH_3NH_3PbI_3$ perovskite + different numbers of layers of PbS QDs (the co-sensitized devices) and those of either individual PbS QDs or $CH_3NH_3PbI_3$ perovskite device are summarized in Table 1. The results show clearly that the best photovoltaic performance was achieved upon co-sensitization with the system composed of $CH_3NH_3PbI_3$ perovskite + 3 layers of PbS QDs. The performance of the $CH_3NH_3PbI_3$ perovskite + 3 layers of PbS QD device improved mainly due to the enhancement in the current density to yield 24.63 mA cm^{-2}. In the case of 1 layer of PbS QDs almost

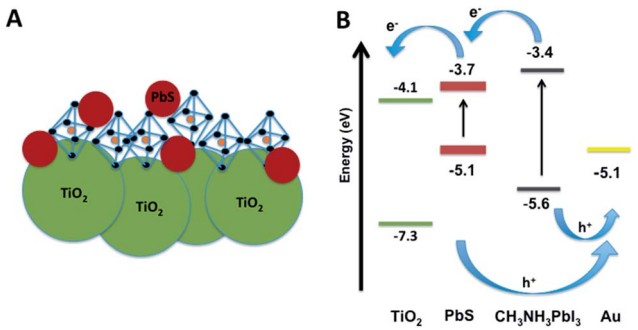

Fig. 1 (A) Schematic representation of the hybrid perovskite PbS QD heterojunction solar cell. (B) Energy level diagram of the components involved in the cell.

Table 1 Summary of the photovoltaic parameters for the different cells

Cell type	J_{sc} (mA cm^{-2})	V_{oc} (mV)	FF	η (%)
$CH_3NH_3PbI_3$	8.33	665.3	0.55	3.04
$CH_3NH_3PbI_3$ + 1 layer PbS QDs	8.6	471	0.5	2.06
$CH_3NH_3PbI_3$ + 3 layer PbS QDs	24.63	343.8	0.43	3.6
$CH_3NH_3PbI_3$ + 6 layer PbS QDs	11	588.8	0.47	2.9
3 layer PbS QDs	0.077	211	0.29	0.004

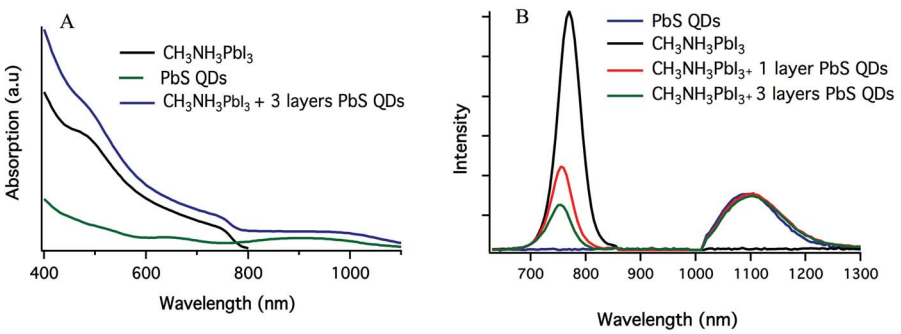

Fig. 2 (A) Absorption spectra on the TiO_2 NP film of the PbS QDs, lead iodide perovskite and lead iodide perovskite with 3 layers of PbS QDs. (B) Emission spectra of the PbS QDs, lead iodide perovskite and lead iodide perovskite with 3 layers of PbS QDs.

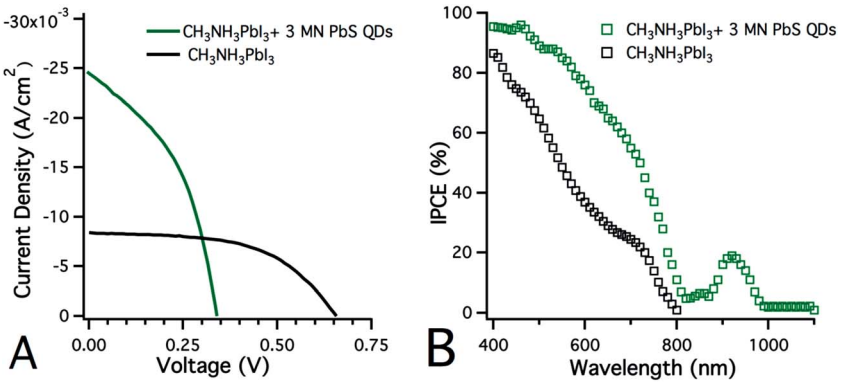

Fig. 3 (A) J–V measurements of the lead iodide perovskite heterojunction solar cell and the hybrid PbS QD lead iodide perovskite heterojunction solar cell. (B) The IPCE of the same heterojunction solar cells.

no contribution in the Near Infra-Red (NIR) region from the PbS QDs occurs, therefore a small enhancement in the J_{sc} was observed, when 6 layers of PbS QDs were deposited some of the perovskite was removed from the surface which affected the J_{sc} of the device, finally the deposition of 3 layers of PbS QDs on the perovskite results in the best photovoltaic performance. The main advantage in co-sensitization is to extend the absorption region of the solar cell, in this study the hybrid perovskite-QD structure has an additional advantage. The inorganic halide atoms in the $CH_3NH_3PbI_3$ perovskite could remove the dangling bonds caused by the excess Pb at the surface of the PbS QDs and in addition passivate the surface states of the QDs. These result in better stability and suppress surface trapping of the PbS QDs.

The current–voltage characteristics and the corresponding IPCE spectra are shown in Fig. 3A and B, respectively. For the co-sensitized system, the enhancement of J_{sc} is understandable from the IPCE spectra; the contribution of the PbS QDs to the NIR region can be observed in addition to the enhancement in the visible region where both materials absorb light. As a result, J_{sc} of the co-sensitized device increased from 8.33 mA cm^{-2} to 24.63 mA cm^{-2} resulting in three times enhancement of the current and an 18% increase in the overall performance. From the current–voltage and EQE spectra, we can infer that the PbS/$CH_3NH_3PbI_3$/mp-TiO_2 solar cell device delivers a photovoltaic response from both the materials. The enhanced device efficiency is attributed to the charge injection occurring from both the sensitizers and to some extent possible energy transfer from high energy perovskite to the lower energy PbS QDs. What is astonishing is 24.63 mA cm^{-2} extracted current demonstrating charge collection efficiency of these materials. The open circuit potential and the fill factor are low, which we optimized by using different linker molecules to adsorb PbS QDs.

Conclusions

This work reports for the first time on co-sensitization between lead iodide perovskite and PbS QDs in a heterojunction solar cell. As a result of this co-sensitization the photocurrent density increased, achieving more than 24 mA cm^{-2}. The co-sensitization opens the possibility to achieve a high absorption of the perovskite in the visible region and to have the NIR contribution of the PbS QDs. The fact that the individual perovskite solar cell already demonstrated high efficiency (using its visible absorption spectra) opens up new avenues for future development of high efficiency photovoltaic cells when increasing the V_{oc} and FF through control of the binding between the two sensitizers could result in a power conversion efficiency as high as 18%.

Experimental

Method and device fabrication

Colloidal PbS QDs capped with oleic acid were purchased from Evident technologies and stored in a nitrogen-filled glove box.

CH_3NH_3I was synthesized by reacting 30 mL methylamine (40% in methanol, TCI) and 32.3 mL of hydroiodic acid (57 wt% in water, Aldrich) in a 250 mL round bottomed flask at 0 °C for 2 h with stirring. The precipitate was recovered by putting the solution on a rotavap and carefully removing the solvents at 50 °C. The yellowish raw product of methylammonium iodide (CH_3NH_3I) was washed with diethyl ether by stirring the solution for 30 min, a step which was repeated three times, and then finally recrystallized from a mixed solvent of diethyl ether and ethanol. After filtration, the solid was collected and dried at 60 °C in a vacuum oven for 24 h.

Device fabrication – thin dense TiO_2 layers of ~100 nm thickness were deposited onto a SnO_2:F conducting glass substrate (15 Ω cm^{-1}, Pilkington) by the spray pyrolysis method.[34] The deposition temperature of the TiO_2 compact layer was 450 °C. TiO_2 nanoparticles films of ~0.5 μm thickness were spin-coated onto this substrate. The TiO_2 layer was annealed at 500 °C for 30 min in air. The substrate was immersed in 40 mM $TiCl_4$ aqueous solutions for 30 min at 70 °C and washed with distilled water and ethanol, followed by annealing at 500 °C for 30 min in air.

The synthesis of $CH_3NH_3PbI_3$ on the TiO_2 surface was carried out by dropping a 40 wt% precursor solution of equimolar CH_3NH_3I and PbI_2 in γ-butyrolactone onto the TiO_2 film. Film formation was induced by spin coating (2000 rpm, 30 s) under glove box conditions. The film coated on the TiO_2 film changed color upon drying at room temperature, indicating the

formation of $CH_3NH_3PbI_3$ in the solid state. The $CH_3NH_3PbI_3$ film was annealed under argon for 15 min at 100 °C.

Following the $CH_3NH_3PbI_3$ film deposition, PbS QDs with their original ligands (oleic acid) were deposited by spin coating on top of the $CH_3NH_3PbI_3$ perovskite.

Finally the counter electrode was deposited by thermal evaporation of gold under a pressure of 5×10^{-5} Torr. The active area was 0.12 cm^2. After the preparation, the cells were allowed to be exposed to air.

Photovoltaic characterization

Photovoltaic measurements employed an AM 1.5 solar simulator equipped with a 450 W xenon lamp (model no. 81172, Oriel). Its power output was adjusted to match AM 1.5 global sunlight (100 mW cm^{-2}) by using a reference Si photodiode equipped with an IR-cutoff filter (KG-3, Schott) in order to reduce the mismatch between the simulated light and AM 1.5 (in the region of 350–750 nm) to less than 2% with measurements verified at two PV calibration laboratories [ISE (Germany), NREL (USA)]. *I–V* curves were obtained by applying an external bias to the cell and measuring the generated photocurrent with a Keithley model 2400 digital source meter. The voltage step and the delay time of the photocurrent were 10 mV and 40 ms, respectively. A similar data acquisition system was used to determine the monochromatic incident photon-to-electric current conversion efficiency. Under full computer control, light from a 300 W xenon lamp (ILC Technology, U.S.A.) was focused through a Gemini-180 double monochromator (Jobin Yvon Ltd, U.K.) onto the photovoltaic cell under test. The monochromator was incremented through the visible spectrum to generate the IPCE (λ) as defined by IPCE (λ) = 12 400 ($J_{sc}/\lambda\varphi$), where λ is the wavelength, J_{sc} is the short-circuit photocurrent density (mA cm^{-2}), and φ is the incident radiative flux (mW cm^{-2}). Photovoltaic performance was measured by using a metal mask with an aperture area of 0.12 cm^2. The measurements were preformed under bias light.

References

1 S. Wang, D. B. Mitzi, C. A. Feild and A. Guloy, *J. Am. Chem. Soc.*, 1995, **117**, 5297.
2 A. Kojima, K. Teshima, Y. Shirai and T. Miyasaka, *J. Am. Chem. Soc.*, 2009, **131**, 6050.
3 J. Im, C. Lee, J. Lee, S. Park and N. Park, *Nanoscale*, 2011, **3**, 4088.
4 M. M. Lee, J. Teuscher, T. Miyasaka, T. N. Murakami and H. J. Snaith, *Science*, 2012, **338**, 643.
5 J. Im, J. Chung, S.-J. Kim and N. Park, *Nanoscale Res. Lett.*, 2012, **7**, 353.
6 H.-S. Kim, C.-R. Lee, J.-H. Im, K.-B. Lee, T. Moehl, A. Marchioro, S.-J. Moon, R. Humphry-Baker, J.-H. Yum, J. E. Moser, M. Grätzel and N.-G. Park, *Sci. Rep.*, 2012, **2**, 591.
7 L. Etgar, P. Gao, Z. Xue, Q. Peng, A. K. Chandiran, B. Liu, M. K. Nazeeruddin, M. Grätzel, M. Gratzel and M. Grätzel, *J. Am. Chem. Soc.*, 2012, **134**, 17396.
8 G. E. Eperon, V. M. Burlakov, P. Docampo, A. Goriely and H. J. Snaith, *Adv. Funct. Mater.*, 2014, **24**, 151.
9 P. Qin, A. L. Domanski, A. K. Chandiran, R. Berger, H.-J. Butt, M. I. Dar, T. Moehl, N. Tetreault, P. Gao, S. Ahmad, M. K. Nazeeruddin and M. Grätzel, *Nanoscale.*, 2014, **6**, 1508.
10 M. J. Carnie, C. Charbonneau, M. L. Davies, J. Troughton, T. M. Watson, K. Wojciechowski, H. Snaith and D. A. Worsley, *Chem. Commun.*, 2013, **49**, 7893.
11 S. Ryu, J. H. Noh, N. J. Jeon, Y. C. Kim, W. S. Yang, J. W. Seo and S. Il Seok, *Energy Environ. Sci.*, 2014, DOI: 10.1039/c4ee00762j.
12 N. J. Jeon, H. G. Lee, Y. C. Kim, J. Seo, J. H. Noh, J. Lee and S. Il Seok, *J. Am. Chem. Soc.*, 2014, **136**, 7837–7840.
13 J. Burschka, N. Pellet, S.-J. Moon, R. Humphry-Baker, P. Gao, M. K. Nazeeruddin and M. Grätzel, *Nature*, 2013, **499**, 316.
14 M. Liu, M. B. Johnston and H. J. Snaith, *Nature*, 2013, **501**, 395.
15 W. A. Laban and L. Etgar, *Energy Environ. Sci.*, 2013, **6**, 3249.
16 J. M. Luther, M. Law, M. C. Beard, Q. Song, M. O. Reese, R. J. Ellingson and A. J. Nozik, *Nano Lett.*, 2008, **8**, 3488.
17 W. Ma, J. M. Luther, H. Zheng, Y. Wu and A. P. Alivisatos, *Nano Lett.*, 2009, **9**, 1699.
18 R. Plass, S. Pelet, J. Krueger, M. Grätzel and U. Bach, *J. Phys. Chem. B*, 2002, **106**, 7578.
19 B. Sun, A. T. Findikoglu, M. Sykora, D. J. Werder and V. I. Klimov, *Nano Lett.*, 2009, **9**, 1235.
20 J. M. Luther, M. Law, Q. Song, C. L. Perkins, M. C. Beard and A. J. Nozik, *ACS Nano*, 2008, **2**, 271.
21 S. Zhang, P. W. Cyr, S. A. Mcdonald, G. Konstantatos and E. H. Sargent, *Appl. Phys. Lett.*, 2005, **87**, 233101.
22 B.-R. Hyun, Y.-W. Zhong, A. C. Bartnik, L. Sun, H. D. Abruña, F. W. Wise, J. D. Goodreau, J. R. Matthews, T. M. Leslie and N. F. Borrelli, *ACS Nano*, 2008, **2**, 2206.
23 R. Debnath, J. Tang, D. A. Barkhouse, X. Wang, A. G. Pattantyus-Abraham, L. Brzozowski, L. Levina and E. H. Sargent, *J. Am. Chem. Soc.*, 2010, **132**, 5952.
24 J. M. Luther, J. Gao, M. T. Lloyd, O. E. Semonin, M. C. Beard and A. J. Nozik, *Adv. Mater.*, 2010, **22**, 3704.
25 L. J. Diguna, Q. Shen, J. Kobayashi and T. Toyoda, *Appl. Phys. Lett.*, 2007, **91**, 023116.
26 A. G. Pattantyus-Abraham, I. J. Kramer, A. R. Barkhouse, X. Wang, G. Konstantatos, R. Debnath, L. Levina, I. Raabe, M. K. Nazeeruddin, M. Grätzel and E. H. Sargent, *ACS Nano*, 2010, **4**, 3374.
27 H. Liu, J. Tang, I. J. Kramer, R. Debnath, G. I. Koleilat, X. Wang, A. Fisher, R. Li, L. Brzozowski, L. Levina and E. H. Sargent, *Adv. Mater.*, 2011, **23**, 3832.
28 J. Gao, J. M. Luther, O. E. Semonin, R. J. Ellingson, A. J. Nozik and M. C. Beard, *Nano Lett.*, 2011, **11**, 1002.
29 J. Gao, C. L. Perkins, J. M. Luther, M. C. Hanna, H.-Y. Chen, O. E. Semonin, A. J. Nozik, R. J. Ellingson and M. C. Beard, *Nano Lett.*, 2011, **11**, 3263.
30 D. A. R. Barkhouse, R. Debnath, I. J. Kramer, D. Zhitomirsky, A. G. Pattantyus-Abraham, L. Levina, L. Etgar, M. Grätzel and E. H. Sargent, *Adv. Mater.*, 2011, **23**, 3134.

31 X. Wang, G. I. Koleilat, J. Tang, H. Liu, I. J. Kramer, R. Debnath, L. Brzozowski, D. A. R. Barkhouse, L. Levina, S. Hoogland and E. H. Sargent, *Nat. Photonics*, 2011, **5**, 480.
32 K. S. Leschkies, T. J. Beatty, M. S. Kang, D. J. Norris and E. S. Aydil, *ACS Nano*, 2009, **3**, 3638.
33 L. Etgar, W. Zhang, S. Gabriel, S. G. Hickey, M. K. Nazeeruddin, A. Eychmüller, B. Liu and M. Grätzel, *Adv. Mater.*, 2012, **24**, 2202.
34 L. Etgar, T. Moehl, S. Gabriel, S. G. Hickey, A. Eychmüller and M. Grätzel, *ACS Nano*, 2012, **6**, 3092.
35 A. H. Ip, S. M. Thon, S. Hoogland, O. Voznyy, D. Zhitomirsky, R. Debnath, L. Levina, L. R. Rollny, G. H. Carey, A. Fischer, K. W. Kemp, I. J. Kramer, Z. Ning, A. J. Labelle, K. W. Chou, A. Amassian and E. H. Sargent, *Nat. Nanotechnol.*, 2012, **7**, 577–582.